



Cite this: DOI: 10.1039/c8ce01418c

Construction of functional coordination polymers derived from designed flexible bis(4-carboxybenzyl)amine†

 Xiutang Zhang, * Hongtai Chen, Bin Li, Guangzeng Liu and Xinzheng Liu

Four coordination polymers (CPs), $[Zn_2(H_2BCA)_2(o\text{-bimb})_2(H_2O)_2]_n$ (**1**), $\{[Pb(H_2BCA)(p\text{-bib})_{0.5}]\cdot H_2O\}_n$ (**2**), $\{[Cd_2(H_2BCA)_2(p\text{-bib})_2]\cdot (H_2O)_3\}_n$ (**3**) and $\{[Zn(H_2BCA)(m\text{-bib})]\cdot H_2O\}_n$ (**4**), have been derived from the designed flexible bis(4-carboxybenzyl)amine (H_2BCA) with bis(imidazole) linkers ($p\text{-bib}$ = 1,1'-benzene-1,4-diylbis(1*H*-imidazole), $m\text{-bib}$ = 1,3-bis(1-imidazolyl)benzene, and $o\text{-bimb}$ = 1,2-bis(imidazol-1-ylmethyl)benzene). X-ray single crystal diffraction analyses reveal that complex **1** is a 3D supramolecular structure composed of 2D 3-connected hcb layers *via* hydrogen contacts. Complex **2** exhibits a 3D 2-nodal (4,5)-connected $\{4^4.6^2\}\{4^4.6^6\}$ -tcs net. Complex **3** shows a novel 2-nodal 3D (4,5,5)-connected net with the point symbol $\{4.6^6.8^3\}_2\{4^2.6^2.8^2\}$. Complex **4** displays a 3D 3-fold interpenetrating 3-connected $\{10^3\}$ ThSi2 net. Structural comparison reveals that the central ions as well as the auxiliary ligand play critical roles in determining the coordination modes of H_2BCA and the final structures. In addition, the luminescence measurements of two zinc-containing compounds (**1** and **4**) have been discussed and show excellent selectivity and sensitivity in detecting acetone molecules and $Cr_2O_7^{2-}/CrO_4^{2-}$ anions in aqueous solution.

 Received 22nd August 2018,
Accepted 5th December 2018

DOI: 10.1039/c8ce01418c

rsc.li/crystengcomm

Introduction

Coordination polymers (CPs) as a new type of functional materials have attracted great interest due to their novel topological diversities, special physical or chemical properties, and a wide range of potential uses.^{1–3} With the improvement of the level of industrialization and the development of human social activities, environmental and water pollution have become a major problem.^{4–6} Among these pollutants, a large number of small toxic organic molecules and heavy metal ions have caused a great negative impact on the survival of human beings. Therefore, the effective and rapid detection of these pollutants is crucial to environmental safety and land security. As a new type of potential functional material, CPs have great applications in the fields of gas adsorption and separation, catalysis and photocatalysis, molecular sensing and fluorescence probing, and so on. Among them, the lumi-

nescent CPs have received great interest because they can be employed for the selective and sensitive detection of environmental pollutants.^{7–9}

Ligand selection is crucial to the synthesis of CPs, and the spatial configurations of the carboxylate ligands have a direct bearing on the structure and the corresponding application properties of the compounds. Depending on whether the configuration of the ligand can be distorted, they can be divided into rigid or flexible ones. Compared with rigid ligands, flexible ligands have stronger deformability, which can adapt to different coordination environments and induce diverse structures such as holes and interpenetrating structures,¹⁰ while carboxylate ligands are considered to be excellent structural constructors and mostly used to construct coordination polymers due to their versatile coordination modes.¹¹ Bis(4-carboxybenzyl)amine (H_2BCA) has a unique $-C-NH-C-$ flexible group. The H_2BCA ligand can rotate freely around a C atom of its own, which is adaptable to more environments in the process of self-assembly with metal ions.

Inspired by the above-mentioned points and following our recent research, we have synthesized a flexible ligand, bis(4-carboxybenzyl)amine (H_2BCA), and used it to react with transition metal ions with bis(imidazole) linkers as auxiliary ligands, finally resulting in four CPs with distinct structures ranging from a 2D 3-connected hcb layer for **1**, a 3D (4,5)-connected tcs net for **2**, a 3D novel (4,5,5)-connected net for **3** and 3D 3-fold interpenetrated 3-connected ThSi2 nets for **4**.

Advanced Material Institute of Research, College of Chemistry and Chemical Engineering, Qilu Normal University, Jinan, 250013, China.

E-mail: xiutangzhang@163.com

† Electronic supplementary information (ESI) available: Additional figures, powder XRD patterns, TG curves, and X-ray crystallographic data. CCDC 1568821 for **1**, 1568819 for **2**, 1568822 for **3**, and 1568820 for **4**. For ESI and crystallographic data in CIF or other electronic format see DOI: 10.1039/c8ce01418c

‡ Current address: Department of Chemistry, College of Science, North University of China, Taiyuan 030051, China.

Luminescence investigations of **1** and **4** indicated that they are efficient blue emission materials, which show excellent selectivity and sensitivity in detecting acetone molecules and $\text{Cr}_2\text{O}_7^{2-}/\text{CrO}_4^{2-}$ anions in aqueous solution.

Experimental section

Materials and methods

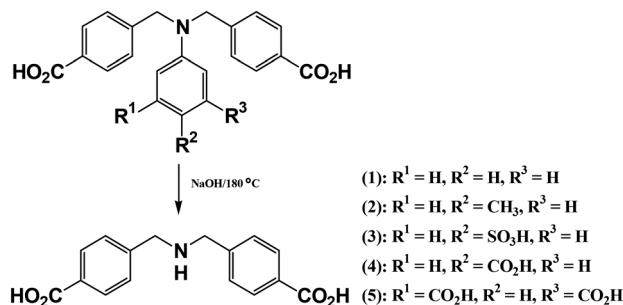
The raw materials for the synthesis of bis(4-carboxybenzyl)-amine and a series of bis(imidazole) ligands were purchased from Jinan Henghua Sci. & Tec. Co. Ltd. and were used without further purification. Elemental analyses were carried out on a Vario MACRO cube elemental analyzer. TGA was carried out from 25 to 700 °C on a ZCTA analyzer at a heating rate of 10 °C min^{-1} under air atmosphere. X-ray powder diffractions of the title compounds were measured on a Rigaku D/Max-2500 PC diffractometer with $\text{Mo-K}\alpha$ radiation over the 2θ range of 5–50° at room temperature. Fluorescence spectra were recorded on a Hitachi F-4600 FL spectrophotometer at room temperature.

Synthesis of *N,N'*-bis(4-carboxybenzyl)amine (H_2BCA)

A mixture of (1)–(5) (0.10 mol) (Scheme 2), 20 g NaOH, and 200 mL H_2O was sealed in an autoclave and heated to 180 °C for one night. The cooled solution was acidified and filtered. White powder was obtained with a yield of 50–70%. EI-MS: m/z $[\text{M} - \text{H}]^-$, 284.10 (calcd for $\text{C}_{16}\text{H}_{15}\text{NO}_4$, 285.10). Anal. (%) calcd. for $\text{C}_{16}\text{H}_{15}\text{NO}_4$, C, 67.36; H, 5.30; N, 4.91. Found: C, 67.25; H, 5.18; N, 4.81. The ^1H NMR data of the designed H_2BCA ligand are shown in Fig. S9.†

Preparation of $\{[\text{Zn}(\text{H}_2\text{BCA})(m\text{-bib})]\cdot\text{H}_2\text{O}\}_n$ (**1**)

A mixture of H_2BCA (0.17 mmol, 0.050 g), *m*-bib (0.20 mmol, 0.042 g), $\text{ZnSO}_4\cdot 7\text{H}_2\text{O}$ (0.20 mmol, 0.057 g), NaOH (0.10 mmol, 0.0040 g), 3 mL DMF, 3 mL methanol and 6 mL H_2O



Scheme 2 The route for the synthesis of H_2BCA .

in a 25 mL Teflon-lined stainless steel vessel was put into an oven at 120 °C for 3 days and then cooled to room temperature slowly. Colourless block crystals of **1** were obtained with a yield of *ca.* 76% (based on H_2BCA). Anal. calcd. for $\text{C}_{28}\text{H}_{25}\text{N}_5\text{O}_5\text{Zn}$: C, 58.29; H, 4.37; N, 12.14 (%). Found: C, 58.68; H, 4.02; N, 12.75 (%).

Preparation of $\{[\text{Pb}(\text{H}_2\text{BCA})(p\text{-bib})_{0.5}]\cdot\text{H}_2\text{O}\}_n$ (**2**)

A mixture of H_2BCA (0.17 mmol, 0.050 g), *p*-bib (0.20 mmol, 0.042 g), $\text{Pb}(\text{OAc})_2\cdot 3\text{H}_2\text{O}$ (0.20 mmol, 0.065 g), NaOH (0.30 mmol, 0.012 g), 3 mL DMF, 3 mL methanol and 6 mL H_2O in a 25 mL Teflon-lined stainless steel vessel was put into an oven at 120 °C for 3 days and then cooled to room temperature slowly. Colourless block crystals of **2** were obtained with a yield of *ca.* 69% (based on H_2BCA). Anal. calcd. for $\text{C}_{44}\text{H}_{40}\text{N}_6\text{O}_9\text{Pb}_2$: C, 43.63; H, 3.33; N, 6.94 (%). Found: C, 44.21; H, 3.18; N, 6.84 (%).

Preparation of $\{[\text{Cd}_2(\text{H}_2\text{BCA})_2(p\text{-bib})_2]\cdot(\text{H}_2\text{O})_3\}_n$ (**3**)

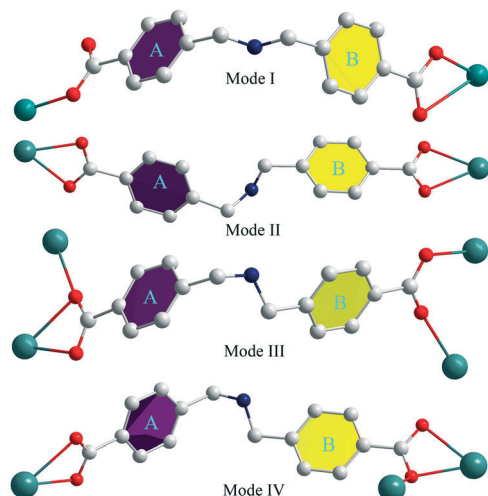
The synthesis process of **3** is similar to that of compound **2** except that $\text{Pb}(\text{OAc})_2\cdot 3\text{H}_2\text{O}$ (0.20 mmol, 0.065 g) was replaced by $\text{GdSO}_4\cdot 8/3\text{H}_2\text{O}$ (0.20 mmol, 0.051 g). Colourless flake crystals of **3** were obtained with a yield of *ca.* 45% (based on H_2BCA). $\text{C}_{56}\text{H}_{50}\text{Cd}_2\text{N}_{10}\text{O}_{10}$: C, 53.90; H, 4.04; N, 11.22 (%). Found: C, 53.62; H, 4.31; N, 11.38 (%).

Preparation of $[\text{Zn}_2(\text{H}_2\text{BCA})_2(o\text{-bimb})_2]\cdot(\text{H}_2\text{O})_2$ (**4**)

A mixture of H_2BCA (0.15 mmol, 0.044 g), *o*-bimb (0.30 mmol, 0.071 g), $\text{ZnSO}_4\cdot 7\text{H}_2\text{O}$ (0.30 mmol, 0.086 g), NaOH (0.20 mmol, 0.080 g), 3 mL ethanol and 6 mL H_2O in a 25 mL Teflon-lined stainless steel vessel was put into an oven at 150 °C for 5 days and then cooled to room temperature slowly. Colourless block crystals of **4** were obtained with a yield of *ca.* 69% (based on H_2BCA). Anal. calcd. for $\text{C}_{60}\text{H}_{58}\text{N}_{10}\text{O}_{10}\text{Zn}_2$: C, 59.56; H, 4.83; N, 11.58 (%). Found: C, 58.93; H, 4.96; N, 12.08 (%).

X-ray crystallography

Intensity data collection was carried out on a Siemens SMART diffractometer equipped with a CCD detector using $\text{Mo-K}\alpha$ monochromatized radiation ($\lambda = 0.71073$ Å) at 296 (2)



Scheme 1 The coordination modes of H_2BCA .

K. The absorption correction was based on multiple and symmetry-equivalent reflections in the data set using the SADABS program. The structures were solved by direct methods and refined by full-matrix least-squares using the SHELXTL package.¹² All non-hydrogen atoms were refined anisotropically. Hydrogen atoms except those on water molecules were generated geometrically with fixed isotropic thermal parameters and included in the structure factor calculations. Crystallographic data for compounds 1–4 are given in Table 1. Selected bond lengths and angles for 1–4 are listed in Table S1.† Further details on the crystal structure investigations may be obtained from the Cambridge Crystallographic Data Centre, with the CCDC depository number 1568821 for 1, 1568819 for 2, 1568822 for 3, and 1568820 for 4.

Results and discussion

Structural description of $\{[\text{Zn}(\text{H}_2\text{BCA})(m\text{-bib})]\cdot\text{H}_2\text{O}\}_n$ (1)

Single-crystal X-ray diffraction analyses reveal that compound 1 crystallizes in the monoclinic system with the space group $P2_1/n$. The unit contains one Zn^{II} ion, one H_2BCA ligand, one m -bib ligand, and one free water molecule (Fig. 1a). The Zn^{II} ion is located in a slightly distorted $\{\text{ZnO}_3\text{N}_2\}$ trigonal bipyramidal geometry, completed by three O atoms from two H_2BCA ligands [$\text{Zn}(1)\text{--O}(1) = 1.97(1)$, $\text{Zn}(1)\text{--O}(2) = 2.76(1)$, $\text{Zn}(1)\text{--O}(3) = 1.93(1)$ Å] and two N atoms from two 1,3-bib ligands [$\text{Co}(1)\text{--N}(4) = 2.02(1)$, $\text{Zn}(1)\text{--N}(5\text{B}) = 2.00(1)$ Å], with $\tau_5 = 0.541$ ($\tau_5 = |\gamma - \beta|/60^\circ$, in which β and γ are the two largest bond angles in the five-coordinate compound; here, $\beta = \angle\text{O}(2)\text{Zn}(1)\text{O}(3) = 153.92^\circ$, $\gamma = \angle\text{O}(3)\text{Zn}(1)\text{N}(5\text{A}) = 120.49^\circ$).¹³

In the assembly process of compound 1, the H_2BCA is completely deprotonated and connected with two Zn^{II} ions which adopted $(\eta^1)\text{--}(\eta^2)\text{--}\mu_2$ coordination modes [Mode I, see Scheme 1, with $\alpha = 88.23^\circ$ (α = the dihedral angle between

the two benzene rings)], leaving a 1D snake-like $[\text{Zn}(\text{H}_2\text{BCA})]_n$ chain with the neighbouring $\text{Zn}(1)\cdots\text{Zn}(1)$ distance being 15.69 Å. Meanwhile, two μ^2 - m -bib ligands adopt the *cis*-configuration to bridge two neighbouring chains with the dihedral angles δ and ε being 36.64° and 66.64° (δ and ε correspond to the dihedral angles between the central benzene ring with the two terminal imidazole rings), successfully construct a binuclear $[\text{Zn}_2(\text{H}_2\text{BCA})_2(1,3\text{-bib})_2]$ chain, in which the nearest $\text{Zn}(1)\cdots\text{Zn}(1)$ distance is 9.62 Å, and further extended to a 2D layer structure by sharing the Zn^{II} ions (Fig. 1b).

In order to explore the topology of compound 1, each Zn^{II} ion can act as a 3-c node; the structure of 1 can be simplified into a 3-connected layer with the point symbol $\{6^3\}$ and the topological type being hcb (uninodal.ttd) (Fig. 1c), while the $[\text{Zn}(\text{H}_2\text{BCA})(1,3\text{-bib})]$ units are expanded into a 3D supramolecular structure through hydrogen bonds ($\text{C}(22)\text{--H}(22)\cdots\text{O}(1)$ and $\text{C}(16)\text{--H}(16\text{A})\cdots\text{O}(4)$) (Fig. 1d). The free water molecules lie between layers. Selected hydrogen bond data for compound 1 are shown in Table 3.

Structural description of $\{[\text{Pb}(\text{H}_2\text{BCA})(p\text{-bib})]_{0.5}\cdot\text{H}_2\text{O}\}_n$ (2)

Structural analysis reveals that compound 2 crystallizes in the monoclinic system with the space group $P2_1/n$ and the asymmetric unit consists of one Pb^{II} ion, one H_2BCA ligand, half a p -bib linker, and one lattice water molecule. As shown in Fig. 2a, the Pb^{II} ion is located in a distorted $\{\text{PbO}_5\text{N}\}$ octahedral coordination environment, completed by five carboxyl O atoms from three different H_2BCA ligands [$\text{Pb}(1)\text{--O}(1) = 2.60(2)$ Å, $\text{Pb}(1)\text{--O}(2) = 2.41(2)$ Å, $\text{Pb}(1)\text{--O}(2\text{B}) = 2.87(2)$ Å, $\text{Pb}(1)\text{--O}(4) = 2.34(2)$ Å, and $\text{Pb}(1)\text{--O}(5) = 2.67(2)$ Å] and one N atom from a 1,4-bib linker [$\text{Pb}(1)\text{--N}(2) = 2.51(2)$ Å].

In complex 2, the completely deprotonated H_2BCA ligand adopts the coordination mode of $(\eta^2)\text{--}(\eta^2:\eta^1)\text{--}\mu_3$ (Mode IV,

Table 1 Summary of crystal data and structure refinement parameters for compounds 1–4

Compound	1	2	3	4
Empirical formula	$\text{C}_{28}\text{H}_{25}\text{N}_5\text{O}_5\text{Zn}$	$\text{C}_{44}\text{H}_{40}\text{N}_6\text{O}_9\text{Pb}_2$	$\text{C}_{56}\text{H}_{50}\text{Cd}_2\text{N}_{10}\text{O}_{10}$	$\text{C}_{60}\text{H}_{58}\text{N}_{10}\text{O}_{10}\text{Zn}_2$
Formula weight	576.90	1211.20	1247.86	1209.9
Crystal system	Monoclinic	Monoclinic	Monoclinic	Monoclinic
Space group	$P2_1/n$	$P2_1/n$	$P2_1/c$	$C2$
<i>a</i> (Å)	10.1766(4)	11.7153(5)	22.0684(9)	19.4892(11)
<i>b</i> (Å)	18.0574(8)	7.8003(3)	17.0982(7)	16.7208(10)
<i>c</i> (Å)	15.0263(6)	23.8533(10)	14.8533(6)	19.5898(16)
β (°)	108.4870	96.4710(10)	104.6660(10)	119.827
<i>V</i> (Å ³)	2617.78(19)	2165.90(15)	5422.0(4)	5538.17(6)
<i>Z</i>	4	2	4	4
D_{calcd} (Mg m^{-3})	1.463	1.857	1.529	1.451
μ (mm^{-1})	0.986	7.825	0.853	0.937
θ range (°)	3.7–25.00	2.95–24.99	2.99–25.00	3.18–25.01
Reflections collected	34 336	27 210	71 505	28 105
Data/restraints/parameters	4005/12/376	3812/4/285	9536/7/719	9610/165/721
<i>F</i> (000)	1192	1164	2528	2512
R_{int}	0.0931	0.3666	0.0656	0.1331
R_1 (wR_2) (all data)	$R_1 = 0.0642$, $wR_2 = 0.1188$	$R_1 = 0.0780$, $wR_2 = 0.2051$	$R_1 = 0.0690$, $wR_2 = 0.1695$	$R_1 = 0.1191$, $wR_2 = 0.1849$
Gof	1.002	1.004	1.002	1.066

$$R_1 = \frac{\sum||F_o| - |F_c||}{\sum|F_o|}, wR_2 = \frac{[\sum w(F_o^2 - F_c^2)^2]}{\sum w(F_o^2)^2}]^{1/2}.$$

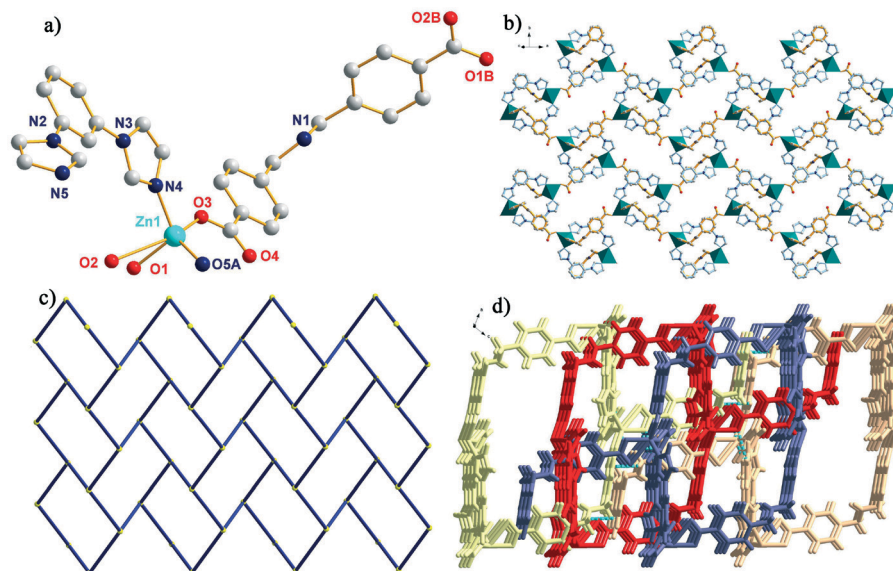


Fig. 1 (a) The coordination environment of Zn^{II} ions in **1** with one free water molecule omitted, (symmetry codes: A: $1 - x, -y, 2 - z$; B: $1.5 + x, 0.5 - y, 0.5 + z$). (b) The 2D layer of compound **1**. (c) The 2D 3-connected hcb layer with the point symbol {6³}. (d) The 3D supramolecular structure by the hydrogen bonds of compound **1**.

Table 2 Structural comparison and discussion of compounds **1–4**

Compound	Coord. mode	Coord. environment	Ancillary ligands/role	Dihedral angle (°) of H ₂ BCA	Structure and topology
1	Mode (I)	{ZnO ₃ N ₂ }	<i>m</i> -Bib/bridging	88.23	2D 3-connected hcb layer
2	Mode (IV)	{PbO ₅ N}	<i>p</i> -Bib/bridging	65.75	3D (4,5)-connected tcs net
3	Mode (II, III)	{CdO ₄ N ₂ }, {CdO ₅ N ₂ }	<i>p</i> -Bib/bridging	65.51	3D novel (4,5,5)-connected net
4	Mode (I)	{ZnN ₂ O ₃ }	<i>o</i> -Bimb/bridging	40.25	3D 3-fold 3-connected ThSi ₂ net

with $\alpha = 65.75^\circ$) to link three Pb^{II} ions and further extends into a 2D [Pb(H₂BCA)]_n fishbone-like polymeric sheet (Fig. 2c) with the Pb1⋯Pb1 distances being 17.11 Å, 14.17 Å, and 4.33 Å. At the same time, the *trans-p*-bib linker acts as a bridge to link two adjacent Pb^{II} ions with the distance of Pb(1)⋯Pb(1) being 14.60(1) Å and the dihedral angles δ and ϵ being 38.14° and 38.14°, respectively, successfully connecting a 2D [Pb(H₂BCA)]_n sheet into a 3D [Pb(H₂BCA)(*p*-bib)_{0.5}]_n framework. The μ^2 -O(2) atom located on the carboxyl group connects two Pb^{II} ions, leaving left- and right-handed [−Pb(1)−O(2)−Pb(1)−]_n helix chains, respectively (Fig. 2b), with \angle Pb(1)O(2)Pb(1) = 109.96° and \angle O(2)Pb(1)O(2) = 131.76°. These two kinds of 1D chiral helical chains can connect as the backbones into a 3D structure through the H₂BCA and 1,4-bib linkers.

From the viewpoint of topology, the Pb^{II} ion can act as a 4-connected node, while the H₂BCA and *p*-bib ligands can be simplified to a 5-connected node. The whole structure can be

described as a 3D 2-nodal 4,5-connected net (Fig. 2d). The point symbol for this net is {4⁴.6²}{4⁴.6⁶}, with the topological type being tcs.

Structural description of [(Cd₂(H₂BCA)₂(*p*-bib)]₂·(H₂O)₃]_n (**3**)

Structural analysis reveals that compound **3** crystallizes in the monoclinic system with the space group *P*₂₁/*c*. The asymmetric unit contains two crystallographically independent Cd^{II} ions, two H₂BCA ligands, two *p*-bib ligands, and three free water molecules. As shown in Fig. 4a, Cd(1) is located in a distorted {CdO₄N₂} octahedral coordination environment, completed by four O atoms (O(5), O(6E), O(7), and O(8)) from three carboxyl groups on three different H₂BCA ligands [Cd(1)−O(5) = 2.26(1) Å, Cd(1)−O(6E) = 2.32(1) Å, Mn(1)−O(7) = 2.44(1) Å, and Cd(1)−O(8) = 2.44(1) Å] and two N atoms from two 1,4-bib linkers [Cd(1)−N(8) = 2.28(1) Å, Cd(1)−N(9) = 2.28(1) Å]. The coordination geometry of Cd(2) is a centrosymmetric {CdO₅N₂} pentagonal bipyramid, which was completed by five O atoms (O(1), O(2), O(3), O(4), and O(4D)) from three carboxyl groups of three H₂BCA ligands [Cd(2)−O(1) = 2.51(1) Å, Cd(2)−O(2) = 2.33(1) Å, Cd(2)−O(3) = 2.38(1) Å, Cd(2)−O(4) = 2.53(1) Å, Cd(2)−O(4E) = 2.33(1) Å], and two N atoms from two distinct 1,4-bib ligands [Cd(2)−N(3) = 2.28(1) Å, Cd(2)−N(5) = 2.29(1) Å].

Table 3 Selected hydrogen bond data for **1**

D−H⋯A	<i>d</i> (H⋯A)/[Å]	<i>d</i> (D⋯A)/[Å]	\angle (D−H⋯A)/[°]
C22−H22⋯O1	2.72	3.38	128
C16−H16A⋯O4	2.78	3.54	135

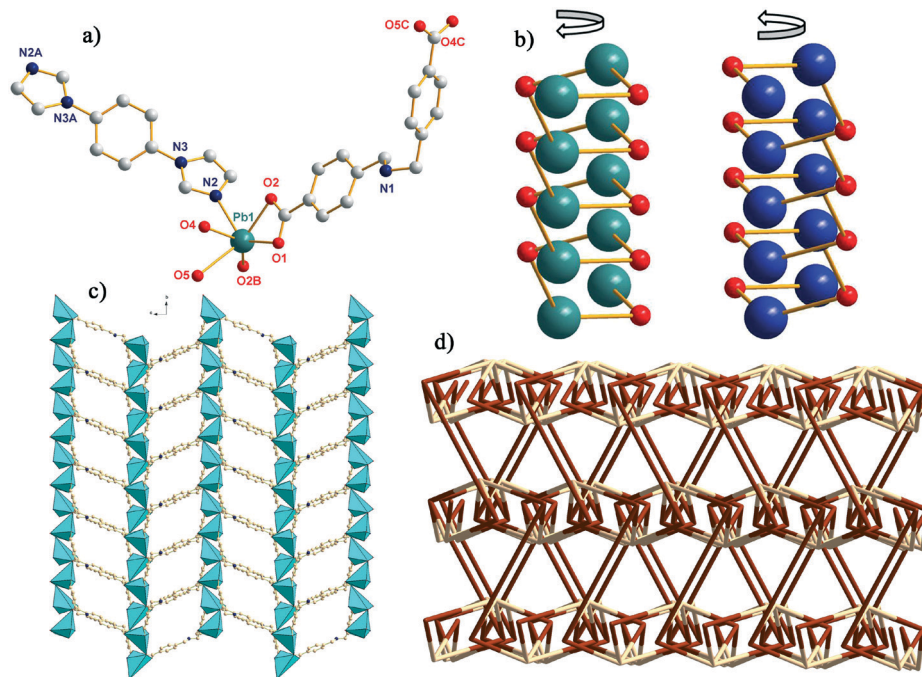


Fig. 2 (a) The coordination environment of Pb^{II} ions in **2** with one free water molecule omitted (symmetry codes: A: $1 - x, 1 - y, 1 - z$; B: $0.5 - x, 0.5 + y, 0.5 - z$; C: $0.5 + x, 0.5 - y, -0.5 + z$). (b) The left- and right-handed $[\text{Pb}(\text{O}^{2-})]_n$ helix chains in **2**. (c) The 2D $[\text{Pb}(\text{H}_2\text{BCA})]_n$ sheet viewed along the a axis of **2**. (d) The 3D 4,5-connected tcs net with the point symbol $\{4^4.6^2\}\{4^4.6^6\}$ of **2**.

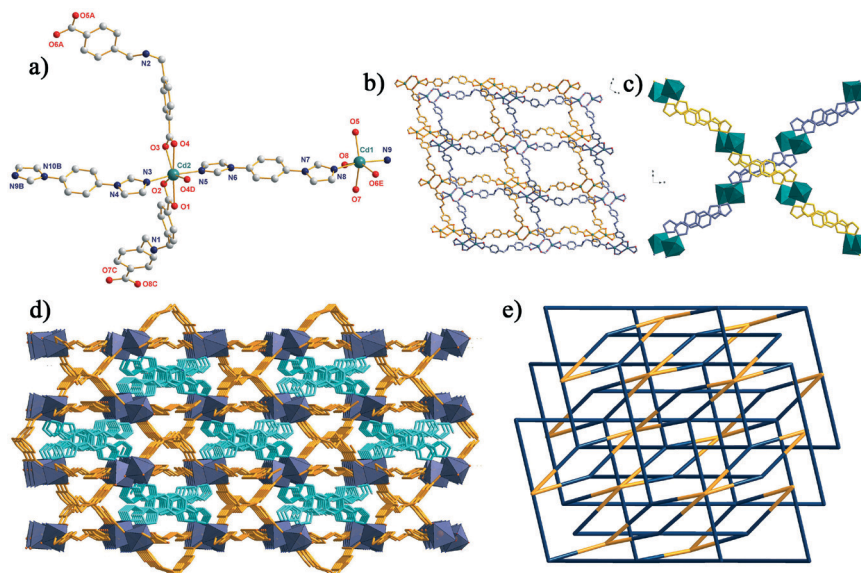


Fig. 3 (a) The coordination environment of Cd^{II} ions in **3** with three water molecules omitted (symmetry codes: A: $1 - x, -0.5 + y, 1.5 - z$; B: $-1 + x, -1 + y, z$; C: $x, 1 - y, -0.5 - z$; D: $1 - x, -y, 1 - z$; E: $2 - x, 1 - y, 1 - z$). (b) The 2D $[\text{Cd}_2(\mu_2\text{-H}_2\text{bca})(\mu_4\text{-H}_2\text{bca})]_n$ sheet in **3** viewed along the b axis. (c) The coordination mode of the 1,4-bib linker in **3** viewed along the c axis. (d) The 3D framework of **3**. (e) The novel 3D 4,5-connected net with the point symbol $\{4.6^6.8^3\}_2\{4^2.6^2.8^2\}$ of **3**.

In compound **3**, the *trans-p*-bib connects Cd(1) and Cd(2) as a linker, leaving two pairs of double-chains with the same structure but extending in different directions (Fig. 3b). The structure of the two single chains which compose the double chain is slightly different (the distances of Cd(1)⋯Cd(2) are 13.91 Å vs. 14.02 Å, and the dihedral angles δ and ϵ are 21.15°

and 12.73° vs. 5.65° and 17.36°), which indicated that the ligand makes the whole structure tend to be stable through the deformation. The completely deprotonated H₂BCA ligand exists with two coordination modes: $(\eta^2)-(\eta^2)-\mu_2$ (Mode II, with $\alpha = 65.51^\circ$ and the distance of Cd(1)⋯Cd(1) being 18.30 Å) and $(\eta^2:\eta^1)-(\eta^1:\eta^1)-\mu_4$ (Mode III, with $\alpha = 83.17^\circ$). As

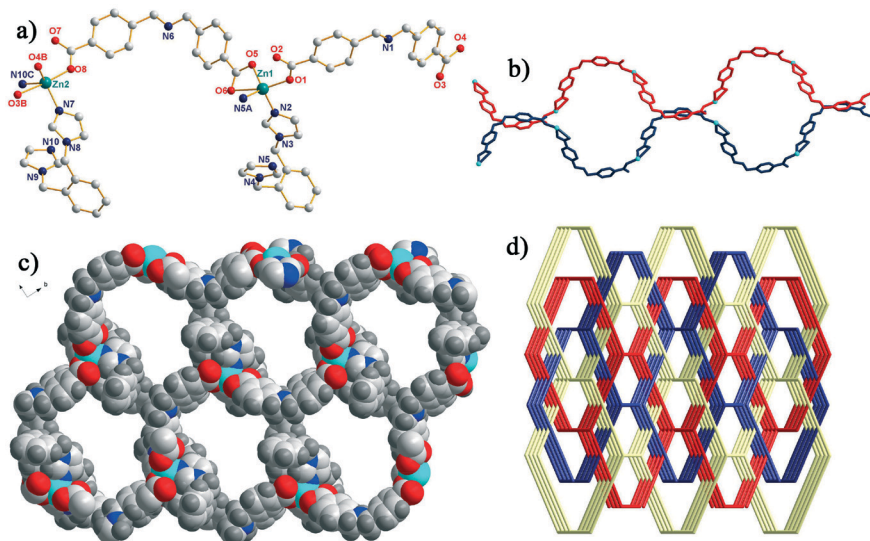


Fig. 4 (a) The coordination environment of Zn^{II} ions in **4** (symmetry codes: A: $-1 - x, y, -z$; B: $0.5 + y, 1.5 + y, z$; C: $-1 - x, y, -1 - z$). (b) The 1D $[\text{Zn}(\text{H}_2\text{BCA})]_n$ polymeric chain viewed along the a axis. (c) The 3D framework of **4**. (d) The 3D 3-fold 3-connected $\{10^3\}$ ThSi2 net of **4**.

shown in Fig. 3b, two H_2BCA ligands with different coordination modes extend in an interlaced direction, leaving a 2D $[\text{Cd}_2(\mu_2\text{-H}_2\text{BCA})(\mu_4\text{-H}_2\text{BCA})]_n$ sheet, and further expanded into a 3D framework by sharing the Cd^{II} ions.

After simplification by using the TOPOS software, the final whole network can be considered as a novel 3D 2-nodal 4,5-connected net with stoichiometry $(4\text{-c})(5\text{-c})_2$, by simplifying the $\{\text{Cd}_2\text{O}_8\text{C}_2\}$ and $\{\text{Cd}_2\text{O}_8\text{C}_2\}$ as two 5-connected nodes, with the point symbol being $\{4.6^6.8^3\}_2\{4^2.6^2.8^2\}$ (Fig. 3e).

Structural description of $[\text{Zn}_2(\text{H}_2\text{BCA})_2(o\text{-bimb})_2(\text{H}_2\text{O})_2]_n$ (**4**)

Crystallographic analysis shows that compound **4** crystallized in the monoclinic system with the space group $C2$. There are two Zn^{II} ions, two H_2BCA ligands, two $o\text{-bimb}$ linkers, and two lattice water molecules in the asymmetric unit of **4** (Fig. 4a). Zn(1) is located in a distorted $\{\text{ZnN}_2\text{O}_3\}$ trigonal bipyramidal geometry with τ_5 being 0.737, surrounded by three O atoms from two different H_2BCA ligands [$\text{Zn}(1)\text{-O}(1) = 1.94(2)$, $\text{Zn}(1)\text{-O}(5) = 1.99(2)$, $\text{Zn}(1)\text{-O}(6) = 2.60(2)$ Å] and two N atoms from two different 1,2- $bimb$ linkers [$\text{Zn}(1)\text{-N}(2) = 1.20(2)$, $\text{Zn}(1)\text{-N}(5A) = 1.98(2)$]. The coordination environment of Zn(2) is similar to that of Zn1 located in a $\{\text{ZnN}_2\text{O}_3\}$ trigonal bipyramidal geometry with the τ_5 being 0.717; the bond length of $\text{Zn}(2)\text{-O/N}$ is in the range of 1.95(2) Å – 2.61(2) Å.

The completely deprotonated H_2BCA ligand acts as a linker to connect two Zn^{II} ions by adopting a $(\eta^1)-(\eta^2)-\mu_2$ mode (Mode I, with α being 40.25°, and the distance of the nearest $\text{Zn}\cdots\text{Zn}$ being 14.48 Å), successfully constructing a 1D $[\text{Zn}(\text{H}_2\text{BCA})]_n$ polymeric chain (Fig. 4b). In addition, two $o\text{-bimb}$ linkers bridge two adjacent Zn^{II} ions by using *trans*-configuration, successfully obtaining a binuclear $[\text{Zn}_2(\text{trans-}o\text{-bimb})_2]$ SBU, with the $o\text{-bimb}$ linker $\text{Zn}\cdots\text{Zn}$ separation distance of 5.33 Å and the dihedral angles δ and ε being 89.943° and 80.89°. Meanwhile, the *trans*-1,4- $bimb$ linkers connect the

Zn^{II} ions on the two nearest 1D $[\text{Zn}(\text{H}_2\text{BCA})]_n$ chains to form the 3D $[\text{Zn}_2(\text{H}_2\text{BCA})_2(o\text{-bimb})_2]_n$ framework.

The topology for **4** was analyzed using the TOPOS program. The Zn^{II} ions can be regarded as a 3-connected node. Therefore, the whole structure can be represented as a 3D 3-fold interpenetrating 3-connected ThSi2 net with the point symbol $\{10^3\}$ (Fig. 4d).

Structural comparison and discussion

From the crystal structures of the four compounds discussed above, we can see that H_2BCA ligands present a variety of coordination modes under similar reaction conditions, with the two deprotonated carboxyl groups coordinating two to four metal ions. As shown in Scheme 1 and Table 2, the H_2BCA ligands in two zinc-based compounds (**1** and **4**) are both connected to two central atoms with the same coordination mode (Mode I) and further extend into a 1D $[\text{Zn}(\text{H}_2\text{BCA})]_n$ chain. These two zinc-containing compounds eventually present different frame structures mainly attributed to the role of auxiliary ligands in the assembly process. Both *m*- bib and *o*- $bimb$ ligands connect two adjacent one-dimensional $[\text{Zn}(\text{H}_2\text{BCA})]_n$ chains, leaving a structure of a 2D 3-connected hcb layer and a 3D 3-connected ThSi2 net, respectively. As a flexible ligand, *o*- $bimb$ has greater deformation capacity in space compared with *m*- bib , which has a more flexible connection to form a high-dimensional structure.¹⁴ For compound **2**, the H_2BCA ligand adopts the coordination mode of $(\eta^2)-(\eta^2:\eta^1)-\mu_3$ (Mode IV) to connect three Pb^{II} ions and further extends into a 2D $[\text{Pb}(\text{H}_2\text{BCA})]_n$ sheet, and *p*- bib further bridges these 2D sheets to form a 3D (4,5)-connected tcs net. Similar to **2**, the *p*- bib ligand of **3** connects two adjacent $[\text{Cd}(\text{H}_2\text{BCA})]_n$ layers to form a 3D (4,5,5)-connected net. Interestingly, the H_2BCA ligands adopt two kinds of coordination modes (Modes II and III) to accommodate two different configurations of Cd^{II} ions.

To the best of our knowledge, all of the coordination modes have never been documented up to now, which also indicates that the selection of central ions has an important influence on the diversity of the H₂BCA coordination mode. In addition, the bis(imidazole) ancillary linkers have a great influence on the final packing structures by modulating their conformations and coordination modes.

Powder X-ray diffraction and thermogravimetric analysis

In order to check the phase purity of these compounds, the PXRD patterns of the title compounds were checked at room temperature. As shown in Fig. S1,[†] the peak positions of the simulated and experimental PXRD patterns are in agreement with each other, demonstrating the good phase purity of the compounds. The dissimilarities in intensity may be due to the preferred orientation of the crystalline powder samples.¹⁵

To investigate the thermal stability of these compounds, thermogravimetric analyses were performed from ambient temperature to 700 °C, and the TG curves are given in Fig. S2.[†] For compound 1, the first weight loss of 3.56% corresponds to the release of lattice water molecules (calcd. 3.44%), and then almost no weight loss is observed until 312 °C, at which temperature it starts to lose the 1,3-bib organic ligand. The final residue is ZnO (found 16.09% and calcd. 15.46%). For 2, the first weight loss in the temperature range of 85–130 °C is consistent with the removal of the coordinated water molecules. Then, the packing structure starts to collapse with the temperature increasing. For 3, the initial weight loss occurs at 90–120 °C, corresponding to the loss of coordinated water molecules. Above 309 °C, the second weight loss corresponds to the loss of the organic ligands. Compound 4 can stably exist until a temperature of up to 387 °C, and then the frameworks decompose gradually, with the final residue being 25.32% (calcd. 23.15% for CdO).

Luminescence properties

The fluorescence spectra of two zinc compounds (1 and 4) and the free H₂BCA, *m*-bib, and *o*-bib ligands were tested in the solid state at room temperature. As can be seen in Fig. S3,[†] emissions of the ligands were observed with wavelengths at 351 nm for *m*-bib, 342 nm for *o*-bib, and 310 nm for the H₂BCA ligand, which may be assigned to π - π^* transitions of the benzene and imidazole rings. Intense emission bands were found at 405 and 407 nm for 1 and 4, respectively ($\lambda_{\text{ex}} = 325$ nm). As the Zn^{II} ion is difficult to oxidize or to reduce due to its d¹⁰ configuration, the emission bands of 1 and 4 are neither metal-to-ligand charge transfer (MLCT) nor ligand-to-metal charge transfer (LMCT) but originate from the intraligand charge transfer because a similar emission was observed for the free H₂BCA ligand. The observed blue shift of the maximum emission bands of the two CPs as compared with that of the free H₂BCA ligand might be attributed to the increased degree of π electron overlap of the organic linkers and the introduction of an auxiliary ligand.¹⁶

Sensing of small organic molecules

In view of the excellent fluorescence properties of these two zinc-containing compounds, we explored the sensing abilities of compounds 1 and 4; methanol, ethanol, DMF, DMA, acetonitrile, *N*-butyl alcohol, and acetone were selected for the luminescence sensing studies. Three milligram samples of 1 and 4 were dispersed in 2 mL diverse solvents with ultrasonication for 30 min. As shown in Fig. 5 and S4,[†] the intensity is in the order methanol > DMA > ethanol > DMF > acetonitrile > *N*-butyl alcohol > acetone (1) and methanol > DMF > DMA > ethanol > acetonitrile > *N*-butyl alcohol > acetone (4). Both 1 and 4 display the strongest luminescence intensity in methanol, while exhibiting the weakest in acetone.

Acetone (Ac) is an important chemical raw material and organic solvent. Therefore, effective and rapid detection of Ac is vital to chemical production and scientific research. The sensing properties of 1 and 4 for Ac were further investigated by monitoring a series of emissions of 1 and 4 in aqueous solutions *versus* gradually increased Ac concentration. As shown in Fig. 6a and S5a,[†] the fluorescence intensity decreased continuously upon incremental addition of Ac into a standard emulsion of 1 and 4 in aqueous solutions. For compound 1, the quenching rate of the emissions reach as much as 95.29% when the concentration of Ac in the suspension solution is 0.235 mM, and 96.35% for compound 4 when the concentration of Ac is 0.260 mM. The I_0/I *versus* the Ac concentration plots are shown in the insets of Fig. 6a and S5a[†] to further quantify the quenching efficiency, where I_0 and I are the fluorescence intensities of the emulsion in the absence and presence of the analyte, respectively. It is notable that the I_0/I *versus* Ac concentration plots bend upwards instead of being typically linear plots; this may be attributed to the presence of simultaneous static and dynamic quenching. Nonlinear Stern-Volmer curves in aqueous systems can be well fitted to the exponential equations $I_0/I = 4.193e^{[Ac]^{0.97583}} - 3.409$ (1) and $I_0/I = 0.052[Ac]^{0.643} + 0.999$ (4), respectively, with a K_{sv} of $3.7 \times 10^4 \text{ M}^{-1}$ (1) and $2.0 \times 10^4 \text{ M}^{-1}$ (4) in the low concentration range. The limits of detection (LODs) of 1 and 4 were found to be as low as 0.09 and 0.13 μM , respectively, which was calculated with the equation $\text{LOD} = 3\delta/S$ (where δ

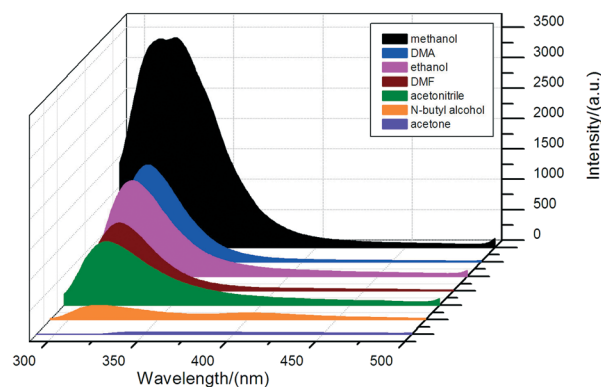


Fig. 5 The luminescence intensities of compound 1 dispersed in different organic solvents.

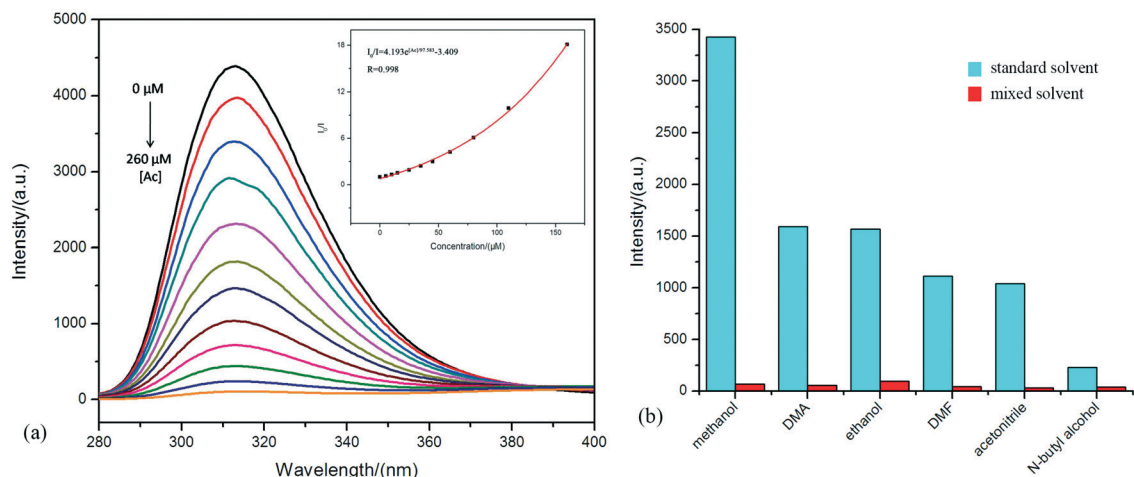


Fig. 6 (a) The PL spectra of the aqueous suspension of compound **1** upon incremental addition of acetone. Inset: The luminescence intensity (I_0/I) versus the acetone concentration. (b) Luminescence intensities of **1** in six different standard solvents or mixed solvents in the presence of acetone.

is the standard deviation of the blank signal and S is the slope of the linear calibration plots). The observed fluorescence quenching may be ascribed to the interactions between the framework and the acetone molecules, in particular, the “C=O” of acetone and the frameworks of **1** and **4**, since such ligand-based fluorescence can be quenched by energy transfer between the organic ligands and the acetone molecules.¹⁷ The different fluorescence sensing performance of complexes **1** and **4** for acetone can be explained as follows: First is the structural difference of complexes **1** and **4**. The H₂BCA ligand adopted different coordination modes in **1** and **4**, and a different auxiliary bis(imidazole) ligand took part in the construction of **1** and **4**. Second, the weak interactions between CPs and acetone molecules may lead to the different orders. Lastly, other factors might be one of the important causes, including electron-withdrawing ability, electrical properties, and vapor pressure of the analytes.

In order to further explore the anti-interference ability of the title compounds for acetone recognition, we studied the sensing abilities of **1** and **4** to different mixed solutions containing acetone. Three milligram samples of **1** and **4** were dispersed in 2 mL of an S/acetone mixed solution in a 1:1 ratio (S = methanol, ethanol, acetonitrile, *N*-butyl alcohol, DMF, or DMA). As can be seen in Fig. 6b and S5b,[†] compared to six standard emulsions based on different solvents, the luminescence intensity of composite emulsions doped with acetone decreased in different degrees. For compound **4**, only the DMF/acetone mixing systems exhibit extremely significant quenching effects on the luminescence of the title CPs, while compound **1** shows a stronger sensing ability for all six mixing systems, and the quenching rates are all more than 90%. The experimental result indicated that compound **1** has excellent anti-interference ability in the identification of acetone.

Selective detection of anions

Meanwhile, to further explore their ability to detect anions of compounds **1** and **4**, as-synthesized samples of **1** or **4** (3 mg)

were ground and dispersed in aqueous solutions containing 12 different Na_{*n*}X with a concentration of [M] = 0.01 M (X = Br⁻, Cl⁻, I⁻, CO₃²⁻, HCO₃⁻, C₂O₄²⁻, SCN⁻, PO₄³⁻, HPO₄²⁻, H₂PO₄⁻, Cr₂O₇²⁻, and CrO₄²⁻) to form an X@1/4 suspension. As shown in Fig. 7, the Cr₂O₇²⁻ and CrO₄²⁻ anions cause the most significant luminescence quenching effects, with the quenching efficiencies being both more than 99%, showing high selectivity.

To obtain a better understanding of the sensing ability of **1** and **4** for the Cr₂O₇²⁻/CrO₄²⁻ anions, a luminescence titration experiment of the 1/4-H₂O suspension was carried out with the gradual addition of an aqueous Cr₂O₇²⁻/CrO₄²⁻ solution. As shown in Fig. 8 and S6,[†] the titration plots revealed that the emission intensities of compounds **1** and **4** decreased with increasing concentrations of the Cr₂O₇²⁻/CrO₄²⁻ anions. The quenching efficiencies of Cr₂O₇²⁻/CrO₄²⁻ (M) to compounds **1** and **4** can be quantitatively rationalized by the equations $I_0/I = 5.828e^{11.540[M]} - 5.028$ (1) and $I_0/I = 0.575e^{31.707[M]} + 0.677$ (4) for Cr₂O₇²⁻ and $I_0/I = 17.945[M] + 1.006$ (1) and $I_0/I = 17.445[M] + 1.017$ (4) for CrO₄²⁻. Obviously, a good linear Stern-Volmer relationship is observed in **1** and **4** for CrO₄²⁻ anion sensing, suggesting that they play a role in the dynamic quenching process for detecting the

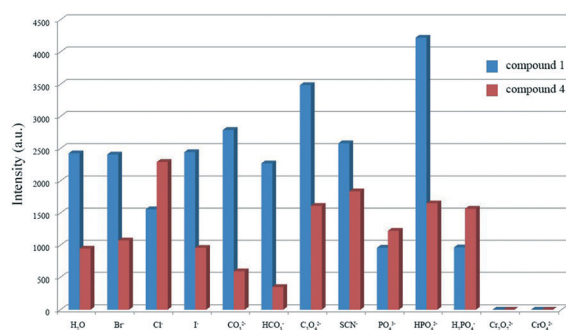


Fig. 7 The luminescence intensities of compounds **1** and **4** in aqueous solution with different anions.

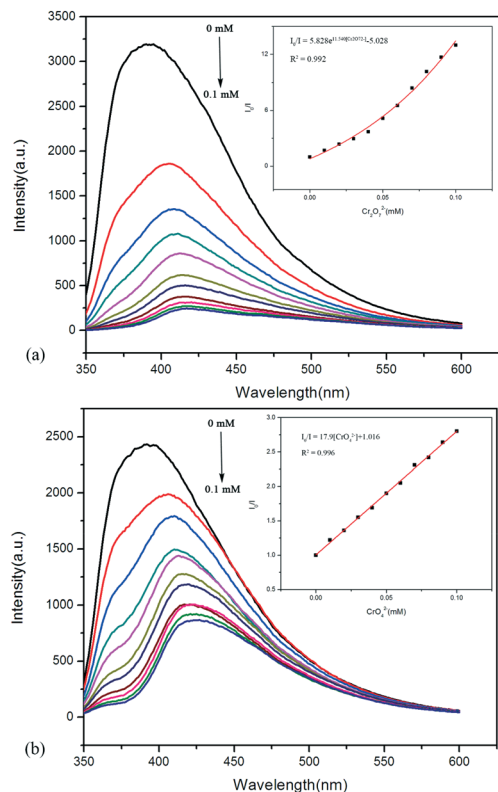


Fig. 8 Luminescence spectra of **1** in an aqueous solution with different concentrations of $\text{Cr}_2\text{O}_7^{2-}$ (a) and CrO_4^{2-} (b). Inset: Luminescence intensity vs. the $\text{Cr}_2\text{O}_7^{2-}/\text{CrO}_4^{2-}$ concentrations plots.

CrO_4^{2-} anion, and the quenching efficiency of $\text{Cr}_2\text{O}_7^{2-}$ can also fit well to the S-V curve in a low concentration range, with a K_{sv} of $6.6 \times 10^4 \text{ M}^{-1}$ (**1**) and $5.3 \times 10^4 \text{ M}^{-1}$ (**4**), respectively. The LODs of CrO_4^{2-} and $\text{Cr}_2\text{O}_7^{2-}$ were estimated to be 0.13 and 0.07 μM for **1**, and 0.14 and 0.07 μM for **4**, respectively. The LODs of CrO_4^{2-} and $\text{Cr}_2\text{O}_7^{2-}$ using **1** and **4** were significantly lower than those observed for other CPs such as $\{[\text{Zn}_2(\text{TPOM})(\text{NH}_2\text{-BDC})_2] \cdot 4\text{H}_2\text{O}\}_n$ (4.8/3.9 μM , TPOM = tetrakis(4-pyridyloxymethylene)methane, $\text{NH}_2\text{-BDC}$ = 2-amino-terephthalic acid),¹⁷ $[\text{Zn}(\text{btz})_n$ (10/2 μM , btz = 1,5-bis(5-tetrazolo)-3-oxapentane), $[\text{Zn}(\text{ttz})\text{H}_2\text{O}]_n$ (20/2 μM , ttz = 1,2,3-tris-[2-(5-tetrazolo)-ethoxy]propane),¹⁸ and $[\text{Zn}(\text{IPA})(\text{L})]_n$ (18.33/12.02 μM , IPA = isophthalic acid, L = 3-pyridylcarboxaldehyde nicotinoylhydrazone).¹⁹ To the best of our knowledge, the quenching efficiency of compounds **1** and **4** is higher than those of most of the previously reported $\text{Cr}_2\text{O}_7^{2-}/\text{CrO}_4^{2-}$ transition metal-based fluorescent probes.¹⁸ To further analyse the recyclability of **1** and **4** as sensors in detecting chromate anions, the quenching effects were tested for three cycles, and no evident reduction was found (Fig. S7†). To investigate the luminescence quenching mechanism caused by $\text{Cr}_2\text{O}_7^{2-}/\text{CrO}_4^{2-}$ anions, PXRD of compounds **1** and **4** after sensing for $\text{Cr}_2\text{O}_7^{2-}/\text{CrO}_4^{2-}$ anions was performed. As shown in Fig. S8† after detecting $\text{Cr}_2\text{O}_7^{2-}/\text{CrO}_4^{2-}$ ions, the skeletons of compounds **1** and **4** remain intact. Hence, the quenching does not result from the collapse of the framework. The selective quenching effect of $\text{Cr}_2\text{O}_7^{2-}/\text{CrO}_4^{2-}$ @1/4 can be explained by

the strong UV-vis absorption bands of the $\text{Cr}_2\text{O}_7^{2-}/\text{CrO}_4^{2-}$ aqueous solution in the range of 230–420 nm,¹⁹ while the other anions' aqueous solutions did not overlap with these absorption ranges. The wide absorption bands of $\text{Cr}_2\text{O}_7^{2-}/\text{CrO}_4^{2-}$ may cover the absorption bands of **1** and **4** upon light excitation. In addition, the quenching effect of $\text{Cr}_2\text{O}_7^{2-}$ @1/4 (in the low concentration) and CrO_4^{2-} @1/4 can well fit the S-V equation, indicating that the quenching effect is attributed to dynamic quenching (collision interaction).²⁰ Hence, the luminescence quenching by $\text{Cr}_2\text{O}_7^{2-}/\text{CrO}_4^{2-}$ anions may be the process involving the competitive absorption upon light excitation and the collision interaction between the $\text{Cr}_2\text{O}_7^{2-}/\text{CrO}_4^{2-}$ anions and the compounds.

Conclusions

In summary, based on the designed flexible ligand of bis(4-carboxybenzyl)amine (H_2BCA), four CPs were obtained, with the structures ranging from a 2D 3-connected hcb layer for **1**, a 3D (4,5)-connected tcs net for **2**, a 3D novel (4,5,5)-connected net for **3** and 3D 3-fold interpenetrated 3-connected ThSi2 nets for **4**. Moreover, luminescence sensing measurements indicate that compounds **1** and **4** both show highly selective and sensitive sensing ability for acetone molecules and $\text{Cr}_2\text{O}_7^{2-}/\text{CrO}_4^{2-}$ anions through fluorescence quenching in aqueous solution, indicating that they are promising candidates for practical applications as chemical sensors.

Conflicts of interest

The authors declare no competing financial interest.

Acknowledgements

This work was financially supported by the National Natural Science Foundation of China (Grant No. 21451001) and the Key Discipline, Innovation Team and Key Lab. of Qilu Normal University.

References

- (a) T. R. Cook, Y. R. Zheng and P. J. Stang, *Chem. Rev.*, 2013, **113**, 734777; (b) P. G. Lassahn, V. Lozan, G. A. Timco, P. Christian, C. Janiak and R. E. P. Winpenny, *J. Catal.*, 2004, **222**, 260–267; (c) T. F. Haselwander, W. Heitz, S. A. Krügel and J. H. Wendorff, *Macromol. Chem. Phys.*, 1996, **197**, 3435–3453; (d) V. C. Gibson and S. K. Spitzmesser, *Chem. Rev.*, 2003, **103**, 283–315; (e) T. R. Younkin, E. F. Conner, J. I. Henderson, S. K. Friedrich, R. H. Grubbs and D. A. Bansleben, *Science*, 2000, **287**, 460–462.
- (a) R. Luebke, Y. Belmabkhout, Ł. J. Weseliński, A. J. Cairns, M. Alkordi, G. Norton, Ł. Wojtas, K. Adil and M. Eddaoudi, *Chem. Sci.*, 2015, **6**, 4095–4102; (b) E. D. Bloch, W. L. Queen, R. Krishna, J. M. Zadrozny, C. M. Brown and J. R. Long, *Science*, 2012, **335**, 1606; (c) T. Devic, C. Serre, N. Audebrand, J. Marrot and G. Férey, *J. Am. Chem. Soc.*, 2005, **127**, 12788–12789.

- 3 (a) H. C. Zhou, J. R. Long and O. M. Yaghi, *Chem. Rev.*, 2012, **112**, 673–674; (b) M. Du, C. P. Li, C. S. Liu and S. M. Fang, *Coord. Chem. Rev.*, 2013, **257**, 1282–1305; (c) X. Zhang, L. Fan, W. Zhang, Y. Ding, W. Fan and X. Zhao, *Dalton Trans.*, 2013, **42**, 16562; (d) U. P. Singh, S. Narang, P. Pachfule and R. Banerjee, *CrystEngComm*, 2014, **16**, 5012.
- 4 (a) B. Wang, A. P. Cote, H. Furukawa, M. O’Keeffe and O. M. Yaghi, *Nature*, 2008, **453**, 207–212; (b) Y. P. He, Y. X. Tan and J. Zhang, *Inorg. Chem.*, 2015, **54**, 6653–6656; (c) X. H. Chang, Y. Zhao, M. L. Han, L. F. Ma and L. Y. Wang, *CrystEngComm*, 2014, **16**, 6417; (d) Z. X. Xu, H. R. Fu, X. Wu, Y. Kang and J. Zhang, *Chem. – Eur. J.*, 2015, **21**, 10236–10240; (e) F. Yu, M. Xiang, A. H. Li, Y. M. Zhang and B. Li, *CrystEngComm*, 2015, **17**, 1556–1563.
- 5 (a) C. Y. Gao, D. Wang, J. P. Li, Y. Wang and W. Yang, *CrystEngComm*, 2016, **18**, 2857–2863; (b) Z. Chen, S. Qin, D. Liu, Y. Shen and F. Liang, *Cryst. Growth Des.*, 2013, **13**, 3389–3395; (c) M. L. Han, X. C. Chang, X. Feng, L. F. Ma and L. Y. Wang, *CrystEngComm*, 2014, **16**, 1687; (d) X. Zhang, J. X. Chen and H. G. Zheng, *Inorg. Chem.*, 2015, **54**, 3183.
- 6 (a) B. Xu, J. Xie, H. M. Hu, X. L. Yang, F. X. Dong, M. L. Yang and G. L. Xue, *Cryst. Growth Des.*, 2014, **14**, 1629–1641; (b) X. X. Jia, R. X. Yao, F. Q. Nagarkar, B. Joarder, A. K. Chaudhari, S. MDai, H. Zhou, X. D. Song, J. J. Zhang, C. Hao, L. Di, Y. X. Wang, J. Ni and H. L. Wang, *CrystEngComm*, 2017, **19**, 2786–2794.
- 7 (a) G. X. Liu, Y. Q. Huang, Q. Chu, T. A. Okamura, W. Y. Sun, H. Liang and N. Ueyama, *Cryst. Growth Des.*, 2008, **8**, 3233–3245; (b) O. V. Magdysyuk, F. Adams, H. P. Liermann, I. Spanopoulos, P. N. Trikalitis, M. Hirscher, R. E. Morris, M. J. Duncan, L. J. McCormick and R. E. Dinnebier, *Phys. Chem. Chem. Phys.*, 2014, **16**, 23908–23914; (c) B. B. Liu, L. Bai, X. L. Lin, K. X. Li, H. Huang, H. L. Hu, Y. Liu and Z. H. Kang, *CrystEngComm*, 2015, **17**, 1686–1692.
- 8 (a) S. Zhang, Q. Yang, X. Y. Liu, X. N. Qu, Q. Wei, G. Xie, S. P. Chen and S. L. Gao, *Coord. Chem. Rev.*, 2016, **307**, 292–312; (b) Z. M. Wang, K. L. Hu, S. Gao and H. Kobayashi, *Adv. Mater.*, 2010, **22**, 1526–1533; (c) L. Zhang, Z. Kang, X. Xin and D. Sun, *CrystEngComm*, 2016, **18**, 193; (d) T. Panda, K. M. Gupta, J. Jiang and R. Banerjee, *CrystEngComm*, 2014, **16**, 4677.
- 9 (a) Y. P. Xia, Y. W. Li, D. C. Li, Q. X. Yao, Y. C. Du and J. M. Dou, *CrystEngComm*, 2015, **17**, 2459–2463; (b) F. Jin, C. Y. Pan, W. X. Zhang, L. Sun, X. Y. Hu, R. B. Liao and D. L. Tao, *J. Lumin.*, 2016, **172**, 264–269; (c) S. H. Wang, F. K. Zheng, M. J. Zhang, Z. F. Liu, J. Chen, Y. Xiao, A. Q. Wu, G. C. Guo and J. S. Huang, *Inorg. Chem.*, 2013, **52**, 10096–10104; (d) R. Wang, X. Liu, A. Huang, W. Wang, Z. Xiao, L. Zhang, F. Dai and D. Sun, *Inorg. Chem.*, 2016, **55**, 1782.
- 10 (a) X. N. Zhang, L. Liu, Z. B. Han, M. L. Gao and D. Q. Yuan, *RSC Adv.*, 2015, **5**, 10119–10124; (b) W. Wang, J. Yang, R. Wang, L. Zhang, J. Yu and D. Sun, *Cryst. Growth Des.*, 2015, **15**, 2589; (c) W. J. Li, J. Lu, S. Y. Gao, Q. H. Li and R. Cao, *J. Mater. Chem. A*, 2014, **2**, 19473.
- 11 (a) B. F. Huang, T. Sun, Z. Sharifzadeh, M. Y. Lv, H. P. Xiao, X. H. Li and A. Morsali, *Inorg. Chim. Acta*, 2013, **405**, 83–90; (b) X. Zhang, Z. J. Wang, S. G. Chen, Z. Z. Shi, J. X. Chen and H. G. Zheng, *Dalton Trans.*, 2017, **46**, 2332.
- 12 (a) G. M. Sheldrick, *SHELXTL*, version 5.1, Bruker Analytical X-ray Instruments Inc., Madison, WI, 1998; (b) G. M. Sheldrick, *SHELX-97*, PC Version, University of Gottingen, Gottingen, Germany, 1997; (c) *SMART, Saint and SADABS*, Bruker AXS Inc., Madison, Wisconsin, USA, 1998.
- 13 (a) V. A. Blatov, A. P. Shevchenko and V. N. Serezhkin, *J. Appl. Crystallogr.*, 2000, **33**, 1193; (b) H. W. Kuai, T. A. Okamura and W. Y. Sun, *Polyhedron*, 2014, **72**, 8–18.
- 14 (a) L. Yang, D. R. Powell and R. P. Houser, *Dalton Trans.*, 2007, 955; (b) D. Banerjee, Z. Hu and J. Li, *Dalton. Trans.*, 2014, **43**, 10668.
- 15 (a) X. Zhang, L. Fan, W. Fan, B. Li, G. Liu, X. Liu and X. Zhao, *CrystEngComm*, 2016, **18**, 6914; (b) L. Fan, W. Fan, B. Li, X. Zhao and X. Zhang, *CrystEngComm*, 2015, **17**, 9413; (c) X. Y. Cao, P. Li, C. X. Li, L. Lv and R. D. Huang, *CrystEngComm*, 2015, **17**, 2398–2405; (d) X. Zhang, L. Fan, W. Fan, B. Li and X. Zhao, *CrystEngComm*, 2015, **17**, 6681.
- 16 (a) X. P. Wang, T. P. Hu and D. Sun, *CrystEngComm*, 2015, **17**, 6681; (b) L. Fan, X. Zhang, Z. Sun, W. Zhang, Y. Ding, W. Fan, L. Sun, X. Zhao and H. Lei, *Cryst. Growth Des.*, 2013, **13**, 2462; (c) M. Dai, X. R. Su, X. Wang, B. Wu, Z. G. Ren, X. Zhou and J. P. Lang, *Cryst. Growth Des.*, 2014, **14**, 240–248; (d) J. Bonnefoy, A. Legrand, E. A. Quadrelli, J. Canivet and D. Farrusseng, *J. Am. Chem. Soc.*, 2015, **137**, 9409–9416.
- 17 (a) B. Chen, L. Wang and F. Zapata, et al, *J. Am. Chem. Soc.*, 2008, **130**, 6718; (b) I. Nawrot, B. Machura and R. Kruszynski, *CrystEngComm*, 2015, **17**, 830–845; (c) Z. Wang, K. K. Tanabe and S. M. Cohen, *Inorg. Chem.*, 2008, **48**, 296; (d) S. Horike, S. Bureekaew and S. Kitagawa, *Chem. Commun.*, 2008, 471; (e) Y. Deng, Z. Y. Yao, P. Wang, Y. Zhao, Y. S. Kang and W. Y. Sun, *Sens. Actuators, B*, 2017, **244**, 114; (f) G. Porter, S. K. Dogra, R. O. Loutfy, S. E. Sugrmore and R. W. Yip, *J. Chem. Soc., Faraday Trans. 1*, 1973, **69**, 1462; (g) R. Lv, J. Wang, Y. Zhang, H. Li, L. Yang, S. Liao, W. Gu and X. Liu, *J. Mater. Chem. A*, 2016, **4**, 15494–15500.
- 18 (a) T. Song, J. Dong, H. Gao, J. Cui and B. Zhao, *Dalton Trans.*, 2017, **46**, 13862–13868; (b) G. Wen, M. Han, X. Wu, Y. Wu, W. Dong, J. Zhao, D. Li and L. Ma, *Dalton Trans.*, 2016, **45**, 15492–15499; (c) Y. Lin, X. Zhang, W. Chen, W. Shi and P. Cheng, *Inorg. Chem.*, 2017, **56**, 11768–11778; (d) X. Zhang, L. Fan, Z. Sun, W. Zhang, D. Li, J. Dou and L. Han, *Cryst. Growth Des.*, 2013, **13**, 792; (e) C. S. Cao, H. C. Hu, H. Xu, W. Z. Qiao and B. Zhao, *CrystEngComm*, 2016, **18**, 4445–4451.
- 19 (a) B. Parmar, Y. Rachuri, K. K. Bisht, R. Laiya and E. Suresh, *Inorg. Chem.*, 2017, **56**, 2627–2638; (b) G. S. Hall, M. J. Angeles, J. Hicks and D. R. Turner, *CrystEngComm*, 2016, **18**, 6614–6623; (c) T. Gu, M. Dai, D. Young, Z. Ren and J. Lang, *Inorg. Chem.*, 2017, **56**, 4668–4678; (d) B. Parmar, Y. Rachuri, K. K. Bisht, R. Laiya and E. Suresh, *Inorg. Chem.*, 2017, **56**, 2627–2638.

- 20 (a) M. A. Kessler, *Anal. Chem.*, 1999, **71**, 1540–1543; (b) G. Hou, Y. Liu, Q. Liu, J. Ma and Y. Dong, *Chem. Commun.*, 2011, **47**, 10731–10733; (c) C. Cao, H. Hu, H. Xu, W. Qiao and B. Zhao, *CrystEngComm*, 2016, **18**, 4445–4451; (d) X. Guo, F. Zhao, J. Liu, Z. Liu and Y. Wang, *J. Mater. Chem. A*, 2017, **5**, 20035–20043; (e) X. Sun, S. Yao, C. Yu, G. Li, C. Liu, Q. Huo and Y. Liu, *J. Mater. Chem. A*, 2018, **6**, 6363–6369.